Journal of Molecular Catalysis A: Chemical 345 (2011) 37–43

Contents lists available at ScienceDirect

Journal of Molecular Catalysis A: Chemical

journal homepage: www.elsevier.com/locate/molcata

A higher energy conformer of (*S*)-proline is the active catalyst in intermolecular aldol reaction: Evidence from DFT calculations

Manjaly J. Ajitha, Cherumuttathu H. Suresh*

Computational Modeling and Simulation Section, National Institute for Interdisciplinary Science and Technology (CSIR), Trivandrum, Kerala, India

ARTICLE INFO

Article history:
Received 19 April 2011
Received in revised form 20 May 2011
Accepted 22 May 2011
Available online 30 May 2011

Keywords:
Organocatalysis
(*S*)-Proline
Aldol reaction
Proton transfer mechanism
Hydrogen bond catalysis
Dispersion-corrected DFT

ABSTRACT

Full catalytic cycle of the stereoselective (*S*)-proline catalyzed aldol reaction of acetone and acetaldehyde in DMSO solvent has been investigated using three different DFT methods, *viz*. B3LYP, MPWB1K and B97D in conjunction with the polarizable continuum (PCM) method. At all the levels of theory, one of the higher energy conformers of the catalyst, **1b** showed higher activity than the most stable conformer, **1a**. On the basis of $\Delta G^{\#}$ of 39.8 kcal/mol observed for the reaction of **1a** with acetone, **1a** is considered to be inactive in the catalytic cycle while the same reaction with **1b** showed 22.7 kcal/mol (B97D-PCM level) lower value for $\Delta G^{\#}$ than **1a**. All the possibilities for enamine formation and C–C bond formation step have been considered for describing the most appropriate stereoselective catalytic cycle which showed that the full cycle is made up of a relay of eight proton transfer steps and the reaction is categorized under hydrogen bond catalysis. The hydration across the iminium bond of the second nucleophilic adduct – an intermediate formed subsequent to the aldehyde addition to the enamine – is the rate limiting step of the reaction with $\Delta G^{\#}$ = 21.7 kcal/mol (B97D-PCM level).

1. Introduction

Asymmetric organocatalysis has been an intense area of research over the past four decades where the main aim is to introduce one or more chiral domains in molecular systems through catalytic activity of small organic molecules [1–13]. The naturally occurring amino acid (*S*)-proline is extensively used as a catalyst for both intramolecular and intermolecular stereoselective aldol reactions [14–18] and in fact, (*S*)-proline catalyzed Hajos–Parrish reaction [19,20] discovered in the 1970s is considered as a prototype of asymmetric catalysis. The high stereoselectivity of this reaction is attributed mainly to the formation of hydrogen bonded transition states [21,22]. Mainly four mechanistic pathways have been proposed for the C–C bond formation step of Hajos–Parrish reaction, (i) the Hajos–Parrish mechanism involving a carbinolamine intermediate (nucleophilic substitution mechanism), (ii) the Hajos–Parrish mechanism involving an enamine intermediate (enaminium-catalyzed mechanism), (iii) the Agami's mechanism [23,24] involving two proline molecules, and (iv) the List's mechanism [15] involving assistance from carboxylic acid of the proline (carboxylic acid-catalyzed enamine mechanism). Transition state modeling at density functional theory (DFT) level by Houk et al. supported mechanism (iv) [25–31], originally put forward by Jung [32] as the most favorable pathway. Further, detailed mechanistic investigation at DFT level has been done by Boyd and co-workers [33,34]. Arno and Domingo [35] studied different possibilities for the diastereoselective C–C bond formation for the intermolecular aldol reaction between acetone and propanaldehyde and found that the *anti-re* attack of the catalyst gives the desired product. Houk et al. established the stereoselectivity and elucidated the complete mechanism of (*S*)-proline catalyzed intramolecular aldol reaction of an achiral triketone [36–38]. Various aspects of all these mechanisms have been reviewed recently [39–50].

Using experimental set up with LA-MB-FTMW spectrometer, very recently Alonso et al. reported extensive conformational studies on (*S*)-proline and identified eight different minimum energy conformers [51,52]. This proves that (*S*)-proline possesses considerable conformational flexibility due to ring flipping and different orientation of the –COOH moiety with respect to the ring nitrogen. Therefore, for a systematic and unbiased approach to organocatalytic reactions, conformational study of the catalyst becomes important to discover the most favorable pathway [53]. Previous mechanistic studies have not addressed this issue of conformational behavior of the catalytically active regions. In this paper, we make such an attempt to describe full mechanistic pathways using different (*S*)-proline conformers and also unambiguously bring out the active role played by a high energy conformation of (*S*)-proline. Further, we will show that the full catalytic cycle can be visualized in terms of a chain of proton transfer pathways involving eight different steps in terms of Gibbs energy profile. The proposed com-

* Corresponding author. Tel.: +91 0471 2515264; fax: +91 0471 2491712.
E-mail address: sureshch@gmail.com (C.H. Suresh).

1381-1169/$ – see front matter © 2011 Elsevier B.V. All rights reserved.
doi:10.1016/j.molcata.2011.05.016

plete proton transfer mechanism is expected to be relevant in the study of aldol reactions catalyzed by enzymes in biological system [54].

2. Computational details

All geometries including the transition state structures were optimized at three different density functional theory (DFT) methods, *viz*. B3LYP/6-31G(d,p), MPWB1K/6-31++G(d,p) and B97D/6-311+G(d,p). B3LYP is a hybrid generalized gradient approximation (GGA) method which incorporates the exact Hartree–Fock exchange and built with the Becke's three-parameter exchange functional (B3) in conjunction with the Lee–Yang–Parr correlation functional (LYP) [55,56]. Although this method is good for main group chemistry [57–59], recent studies pointed out the shortcomings in estimating the barrier heights and modeling noncovalent interactions [60,61]. MPWB1K is a hybrid meta-GGA method formulated by Zhao and Truhlar [62] which has been recently used for making good predictions on thermochemistry, thermochemical kinetics, hydrogen bonding, and weak interactions [63,64]. B97D is a recently developed DFT method by Grimme [65] which includes a semiempirical correction for the treatment of van der Waals (dispersion) interaction. Very recently, this method has been successfully applied for some mechanistic investigations [66–69]. In all the three DFT methods, solvent effects were also included by applying the polarizable continuum model (PCM) of the self consistent reaction field for full optimization [70,71]. To indicate the PCM option, the DFT methods are named as B3LYP-PCM, MPWB1K-PCM and B97D-PCM. Solvent parameters of dimethyl sulphoxide (DMSO) are used in the calculation. The B3LYP-PCM, MPWB1K-PCM calculations were performed using Gaussian 03 [72] and B97D-PCM calculations were performed using Gaussian 09 [73] suite of quantum chemical programs. The UAHF (United Atom Topological Model for Hartree Fock) keyword is specified to build the cavity for PCM calculation which is automatically set by the program according to the molecular topology, hybridization, formal charge, etc. [71]. The transition states (TSs) were located using synchronous transit-guided *quasi*-Newton method (QST3) [74,75]. TSs were characterized by only one imaginary frequency (first order saddle points); relevant to the desired bond-breaking/bond-forming reaction coordinates. Further, IRC calculations were performed to further authenticate the results. Always the relative Gibbs energy (ΔG_{rel}) is reported and the point 0.00 kcal/mol represents the sum of the Gibbs energies of the most stable (*S*)-proline conformation; acetone and acetaldehyde unless otherwise specified. Among the three different methods; the B97D-PCM values were used throughout for discussion unless otherwise mentioned. The details of energy parameters are reported in Supporting information.

3. Results and discussion

3.1. Selection of (S)-proline conformations

Different conformations of (*S*)-proline are depicted in Fig. 1 along with relative Gibbs energy at the three different DFT levels. The most stable conformation is **1a** which is in agreement with the LA-MB-FTMW experimental results [51,52]. Close proximity of the acidic proton and the *N*-lone pair in **1a**, **1b** and **1d** would bring in bi-functionality to the catalyst towards an approaching carbonyl compound by simultaneous attack through *N*-lone pair on the carbonyl carbon and interaction of the acidic proton on the developing alkoxide moiety. Such a bi-functionality is not possible with other conformations. Since **1a** and **1d** differ only in the orientations of the methylene moieties, particularly at the C4 position (up for **1a** and down for **1d**), both would show very similar behavior in mechanistic studies. In a previous study, Houk et al. [39] examined the conformational up (endo) and down (exo) behavior of the C4 center and suggested that the up conformation (**1a**) is generally favored over the down conformation (**1d**) for unsubstituted proline catalysts. Hence, we have considered only **1a** and **1b** for detailed mechanistic studies. In fact, the conformers **1e**, **1f**, **1g**, and **1h** cannot form a transition state for the nucleophilic adduct formation and a transition state search from **1c** will converge to that from **1b** (Supporting information). **1a** is more stable than **1b** by 5.9 kcal/mol at B97D-PCM/6-311+G(d,p) level and possesses a *syn*-orientation for C–H bond of the chiral carbon and the N–H bond of the ring nitrogen, whereas the C–H and the N–H bonds of **1b** exhibit *anti*-orientation. Higher stability of **1a** can be attributed to the intramolecular O–H. . .N hydrogen bond of distance 1.72 Å. The zwitterionic form of the catalyst **1a** (more stable than the neutral **1a** by 0.9 kcal/mol in DMSO solvent) is also modeled which is expected to be catalytically inactive due to the quaternization of the nitrogen center. Since quaternization removes the nucleophilicity of the nitrogen, this tautomer is not considered for the mechanistic studies (Supporting information).

3.2. Initial nucleophilic attack: active form of the catalyst

Using the (*S*)-proline conformations **1a** and **1b**, the nucleophilic attack of the *N*-lone pair on the carbonyl carbon of acetone is investigated. Acetone is preferred rather than aldehyde for the initial reaction because in intermolecular aldol reaction, aldehyde is added slowly to the performed solution of proline and ketone [76] to overcome the side reactions arising from the inability of the catalyst to differentiate between the aldehyde and ketone for the initial nucleophilic attack. The Gibbs energy profiles for the (**1a** + acetone) and (**1b** + acetone) reactions are presented in Figs. 2 and 3, respectively. In the case of **1a**, the pre-reacting complex of the proline and acetone, **2a**, has to pass through the transition state $\mathbf{TS_{1a}}$ (ΔG_{rel} = 20.3 kcal/mol) to reach the zwitterionic intermediate **3a**. The zwitterion to neutral form ($\mathbf{3a} \rightarrow \mathbf{TS_{2a}} \rightarrow \mathbf{4a}$) generates the highest point $\mathbf{TS_{2a}}$ in the Gibbs energy profile (ΔG_{rel} = 39.8 kcal/mol). The activation Gibbs energy barrier ($\Delta G^{\#}$) for this step is 19.3 kcal/mol. Overall, the reaction is endergonic by 30.0 kcal/mol of energy. It is thus clear that this highly endergonic reaction requiring a high value of ΔG_{rel} for $\mathbf{TS_{2a}}$ may not occur at the specified reaction conditions.

Enhancement in catalytic activity is expected when the *N*-lone pair in (*S*)-proline is readily available for the initial nucleophilic attack on the carbonyl carbon. Among all the conformations, the *N*-center has maximum degree of pyramidalization in **1b** (23.2°) which indicate higher nucleophilic character from the localized *N*-lone pair than the other conformations. In **1a**, the lone pair is partially shielded by the O–H. . .N hydrogen bond while **1b** has a more exposed *N*-lone pair. If **1a** can be converted easily to **1b** via a pyramidal inversion at the ring nitrogen, **1b** would play a more active role in the catalysis. The $\Delta G^{\#}$ for **1a** to **1b** conformational change via $\mathbf{TS_{ab}}$ is only 11.0 kcal/mol (Fig. 3). The reaction of **1b** with acetone, passing through a van der Waals complex (**2b**) can yield the zwitterionic intermediate **3b**. This step requires ΔG_{rel} of 17.1 kcal/mol and the associated transition state is $\mathbf{TS_{1b}}$. The geometries of **2b** and $\mathbf{TS_{1b}}$ agree well with the recent report given by Yang et al. [42]. The next step of the reaction is nearly barrier less ($\Delta G^{\#}$ = 1.4 kcal/mol). Thus, even with **1a** as the reference point for proline, the ΔG_{rel} between **1a** and $\mathbf{TS_{1b}}$ is only 17.1 kcal/mol (B97D-PCM) which is 22.7 kcal/mol smaller than the pathway described in Fig. 2 using the transition state $\mathbf{TS_{2a}}$. Further, the pathway passing through the intermediacy of **1b** is endergonic by 14.5 which is 15.5 kcal/mol lower than that of the pathway exclusively via **1a**. However, one may argue that **4a** and **4b** are readily interconvertible due to rotation of the carboxylate group on the pyrrolidine ring, suggesting

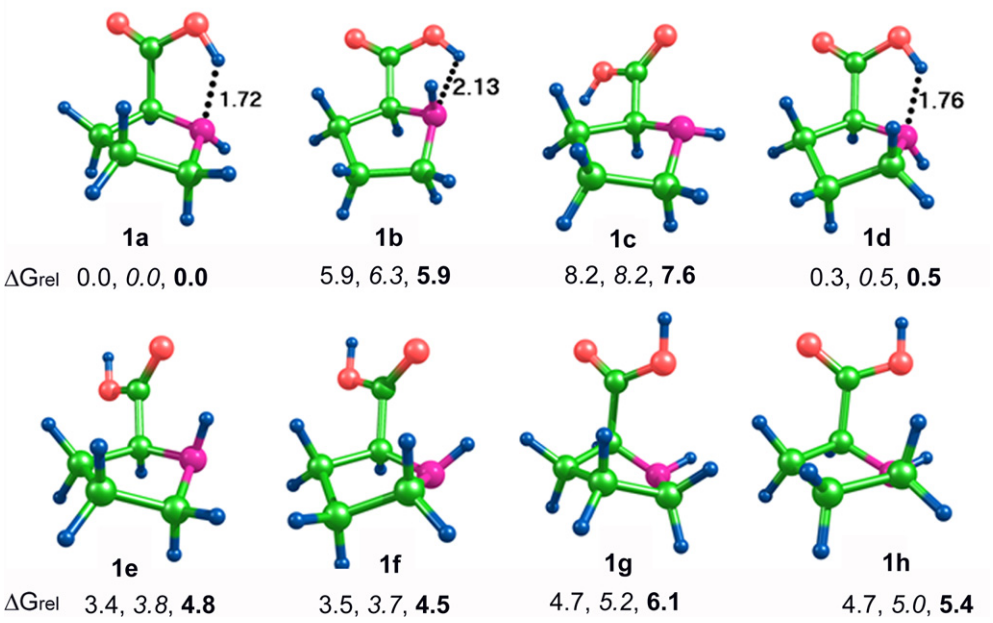

Fig. 1. Different conformers of (*S*)-proline. Numerical values in regular, italics and bold fonts are the relative Gibbs energies (ΔG_{rel}) with respect to the most stable conformer (**1a**) in kcal/mol at B3LYP-PCM, MPWB1K-PCM and B97D-PCM levels respectively. B97D-PCM level structures are given.

pathway in Figs. 2 and 3 will have the same endergonic character. Thus it is clear that pathway in Fig. 2 can be discarded on the basis of the high $\Delta G^{\#}$ of 39.8 kcal/mol observed for $\mathbf{TS_{2a}}$ while pathway in Fig. 3 is the right choice to carry out the reaction which also suggests that **1b** must be the active form of the catalyst and not **1a**. Hence, hereafter we have considered only the subsequent reactions from **4b** (Fig. 3). The higher stability of **4b** than **4a** is due to a strong intramolecular N. . .H hydrogen bond of distance 1.78 Å in **4b** (Fig. 3).

3.3. Formation of the iminium ion and conversion to enamine

Elimination of a water molecule takes place from **4b** (1-(2-hydroxypropan-2-yl)pyrrolidine-2-carboxylic acid) when it passes through $\mathbf{TS_{3b}}$ and forms the zwitterionic iminium ion–water complex **5b** (Fig. 4). At the B97D-PCM level, this step requires $\Delta G^{\#}$ of 3.5 kcal/mol of Gibbs energy while at MPWB1K-PCM level and at B3LYP-PCM levels; the $\Delta G^{\#}$ is 12.9 and 7.5 kcal/mol, respectively. At MPWB1K-PCM and B97D-PCM levels, the product system shows higher stabilization than the reactant while at B3LYP-PCM level, the product and reactant systems show nearly equal Gibbs energy. Further, the binding energy of water in **5b** is 3.6 kcal/mol at B97D-PCM level and 1.6 kcal/mol at MPWB1K-PCM level. At both these levels, the dissociation of water to **6b** is favored due to gain in entropy on the ΔG_{rel} scale. On the other hand, at the B3LYP-PCM level, the dissociation of water molecule is slightly disfavored.

(*S*)-Proline catalysis is widely accepted to undergo enamine pathway [77,78]. Iminium ion can be converted to enamine in four

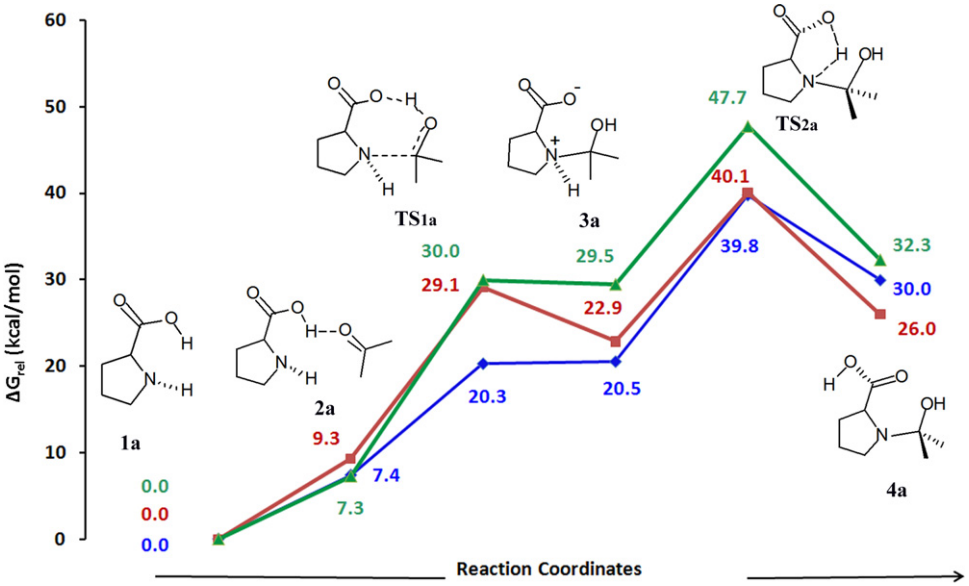

Fig. 2. Energy profile diagram for the initial nucleophilic attack by **1a**. The numerical values are the relative Gibbs energies (ΔG_{rel}) in kcal/mol (B3LYP-PCM values in green, MPWB1K-PCM in red and B97D-PCM in blue colors) with respect to **1a**. (For interpretation of the references to color in this figure legend, the reader is referred to the web version of the article.)

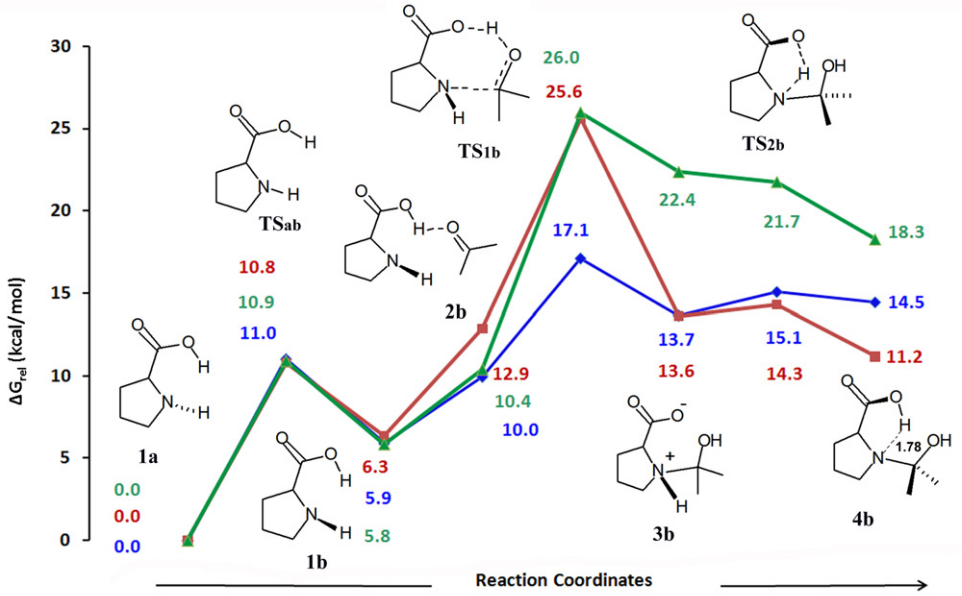

Fig. 3. Energy profile diagram for the initial nucleophilic attack by **1b**. The numerical values are the relative Gibbs energies (ΔG_{rel}) in kcal/mol (B3LYP-PCM values in green, MPWB1K-PCM in red and B97D-PCM in blue colors) with respect to **1a**. (For interpretation of the references to color in this figure legend, the reader is referred to the web version of the article.)

different pathways; two water-assisted and two direct pathways which may give either *syn*-enamine or *anti*-enamine. Hence, we have considered both **5b** and **6b** for further mechanistic investigations. Although the energetics in Fig. 4 is in favor of **6b**, pathway from **5b** also will be useful to verify the role of water. In Fig. 5, the ΔG_{rel} of all the four pathways are depicted. The $\Delta G^{\#}$ for the formation of water-assisted-*syn* enamine via $\mathbf{TS_{4a}}$, water-assisted-*anti*-enamine via $\mathbf{TS_{4c}}$, direct-*syn*-enamine via $\mathbf{TS_{4b}}$ and direct-*anti*-enamine via $\mathbf{TS_{4d}}$ are 23.9, 22.5, 16.2 and 28.0 kcal/mol, respectively (Fig. 5). In general MPWB1K-PCM level $\Delta G^{\#}$ is slightly higher than B97D-PCM values while B3LYP-PCM values are slightly smaller and on the whole, all the three levels agree that the formation of *syn*-enamine (**7b**) without the assistance of water via $\mathbf{TS_{4b}}$ is the most preferred pathway. The product from $\mathbf{TS_{4a}}$, $\mathbf{TS_{4b}}$, $\mathbf{TS_{4c}}$, and $\mathbf{TS_{4d}}$ are respectively **7a** (*syn*-enamine water complex), **7b**, **8a** (*anti*-enamine water complex) and **8b** (*anti*-enamine). All the levels also agree that *anti*-enamine is thermodynamically the most stable structure. Though the preferred pathway leads to **7b**, formation of *anti*-enamine, **8b** can be easily achieved by the N–C bond rotation. The $\Delta G^{\#}$ for the rotation is only 5.2 kcal/mol at B97D-PCM/6-311+G(d,p) level of theory (Supporting information). It may be noted that in $\mathbf{TS_{4a}}$, $\mathbf{TS_{4b}}$, and $\mathbf{TS_{4c}}$, the C4 center shows up conformation while the C4 in $\mathbf{TS_{4d}}$ possesses down conformation. Recently, Houk et al. [39] have mentioned the preference of the up conformation over the down conformation in unsubstituted prolines and suggested that the preferred pathway passes through the up conformation. The present results also agree with their findings.

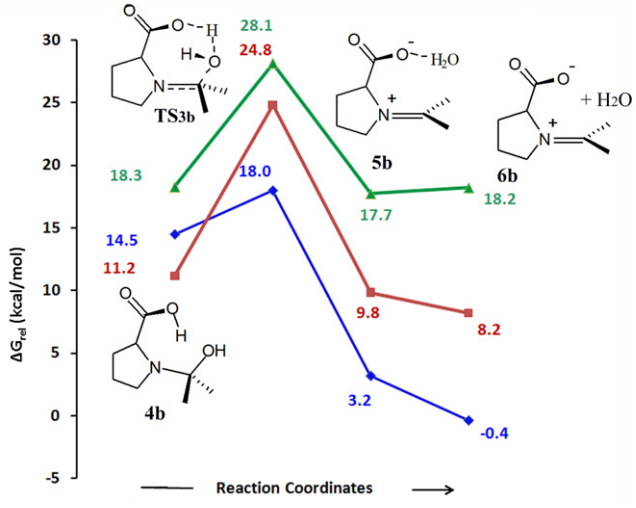

Fig. 4. Energy profile diagram for the formation of iminium ion. The numerical values are the relative Gibbs energies (ΔG_{rel}) in kcal/mol (values of B3LYP-PCM in green, MPWB1K-PCM in red and B97D-PCM in blue colors) with respect to **1a**. (For interpretation of the references to color in this figure legend, the reader is referred to the web version of the article.)

3.4. Second nucleophilic attack (C–C bond formation step)

The second nucleophilic attack of enamine on acetaldehyde is accountable for the C–C bond formation step. Since **7b** and **8b** are nearly iso-energetic and easily interconvertible, both were considered for modeling *si* and *re* facial nucleophilic attack on the carbonyl carbon of the approaching electrophiles. Accordingly, four different diastereomeric pathways for the C–C bond formation, *viz.* the *anti-si* via $\mathbf{TS_{5a}}$, *anti-re* via $\mathbf{TS_{5b}}$, *syn-si* via $\mathbf{TS_{5c}}$, and *syn-re* via $\mathbf{TS_{5d}}$ (Fig. 6) which account for the stereocontrolling step of the reaction. It is interesting to note that all the pathways are Burgi–Dunitz type [79–81] where the nucleophile will attack the carbonyl carbon, forming an angle in the range of 100–110°. Among them, the attack of the acetaldehyde by the *anti*-enamine in a *re*-fashion via $\mathbf{TS_{5b}}$ is the most preferred one ($\Delta G^{\#}$ = 10.4 kcal/mol) which leads to the formation of the product **10b** in the (*S*)-configuration. According to Curtin–Hammett principle, the enantiomeric excess (ee) of the (*S*)-isomer is 40% (Supporting information). In experiments, sterically bulky alkyl and aryl substituted aldehydes have been used and the reported ee fall in the range of 58–96% [82,83]. Since acetaldehyde is sterically not a very demanding system, the reported ee in this work is reasonable.

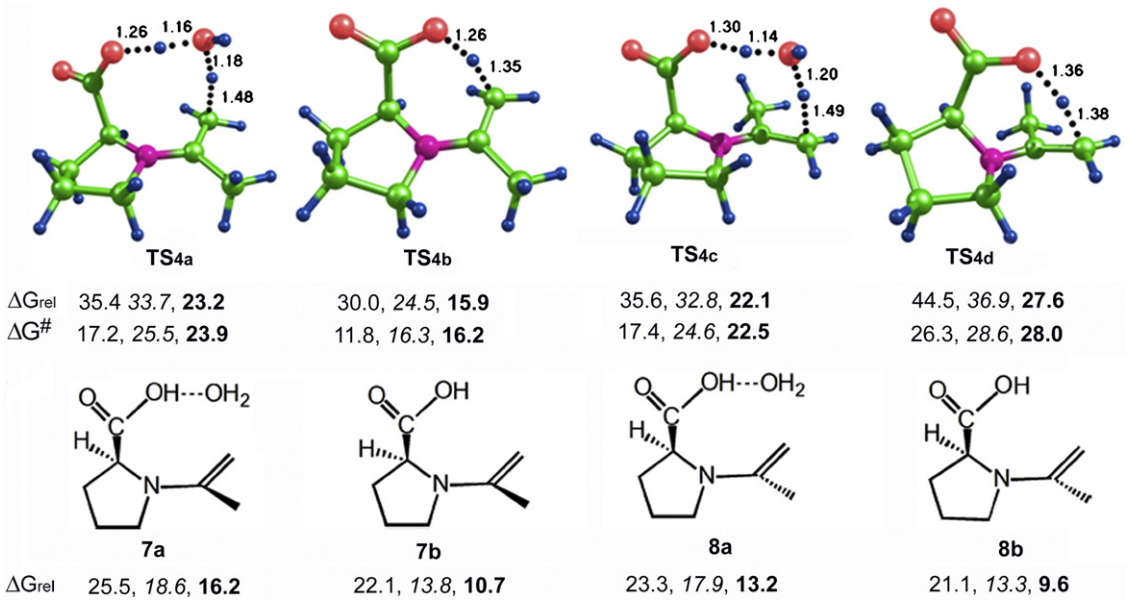

Fig. 5. Transition states for water-assisted and direct pathways of enamine formation and the ensuing products. Numerical values are the relative Gibbs energies (ΔG_{rel}) and activation Gibbs energy barrier ($\Delta G^{\#}$) in kcal/mol (regular, italics and bold fonts are at B3LYP-PCM, MPWB1K-PCM and B97D-PCM levels respectively). **7a** and **7b** are *syn*-enamines and **8a** and **8b** are *anti*-enamines. B97D-PCM level structures are given.

3.5. Regeneration of the catalyst

The product **10b** is zwitterionic and it is expected that the water molecule eliminated from the iminium ion water complex (**5b**) can re-enter into the reaction to form the zwitterionic water complex (**11b**). This leads to the addition of water across the carboxylate group and the unsaturated carbon to form **12b**. The water addition required $\Delta G^{\#}$ of 21.7 kcal/mol. In the next two consecutive steps, rearrangement of protons in COOH and OH moieties occur (**12b** → **TS$_{7b}$** → **13b** → **TS$_{8b}$** → **14b**) giving rise to the formation of **14b** which is a weak complex of the desired product (*S*)-β-hydroxy ketone (**15b**) and (*S*)-proline. Regeneration of the active form of the catalyst (**1b**) takes place with the release of 4.2 kcal/mol of energy (Fig. 7). The regenerated catalyst **1b** is active to keep the catalytic cycle alive.

The complete catalytic cycle of the most probable mechanism described herein passes through eight proton transfer transition states (**TS$_{1b}$**, **TS$_{2b}$**, **TS$_{3b}$**, **TS$_{4b}$**, **TS$_{5b}$**, **TS$_{6b}$**, **TS$_{7b}$** and **TS$_{8b}$**) and they all describe proton transfer from reactant side to product side. The well defined hydrogen bonded frameworks in the transition states provide the driving force for the shuttling of acidic proton from COOH to ketonic/aldehydic CO and also to secondary amine functionality.

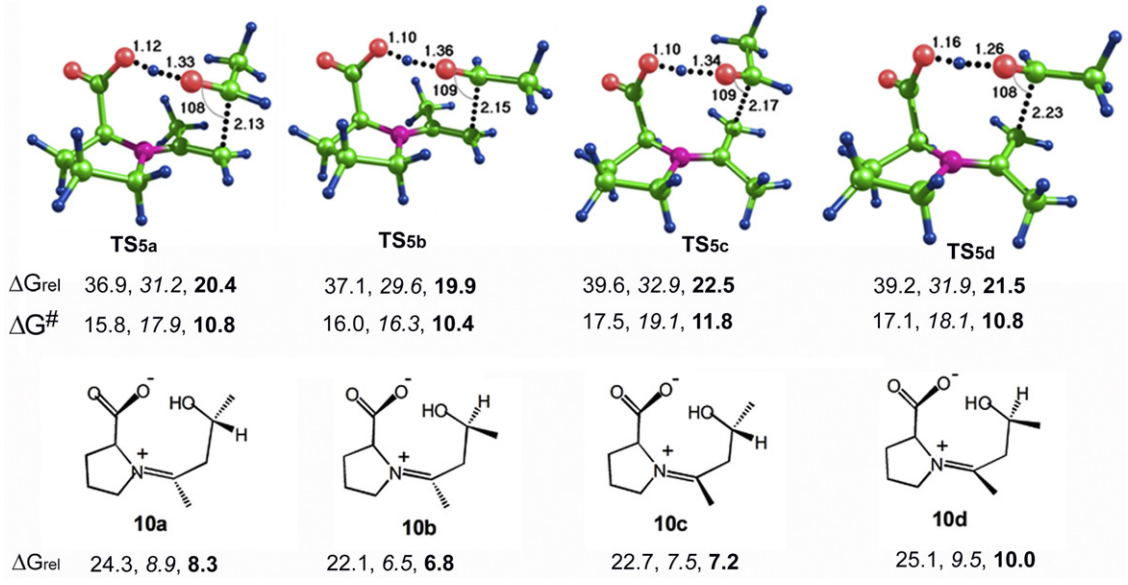

Fig. 6. Transition states for C–C bond formation and the ensuing products. Numerical values are the relative Gibbs energies (ΔG_{rel}) and activation Gibbs energy barrier ($\Delta G^{\#}$) in kcal/mol (regular, italics and bold fonts are at B3LYP-PCM, MPWB1K-PCM and B97D-PCM levels respectively). B97D-PCM level structures are given.

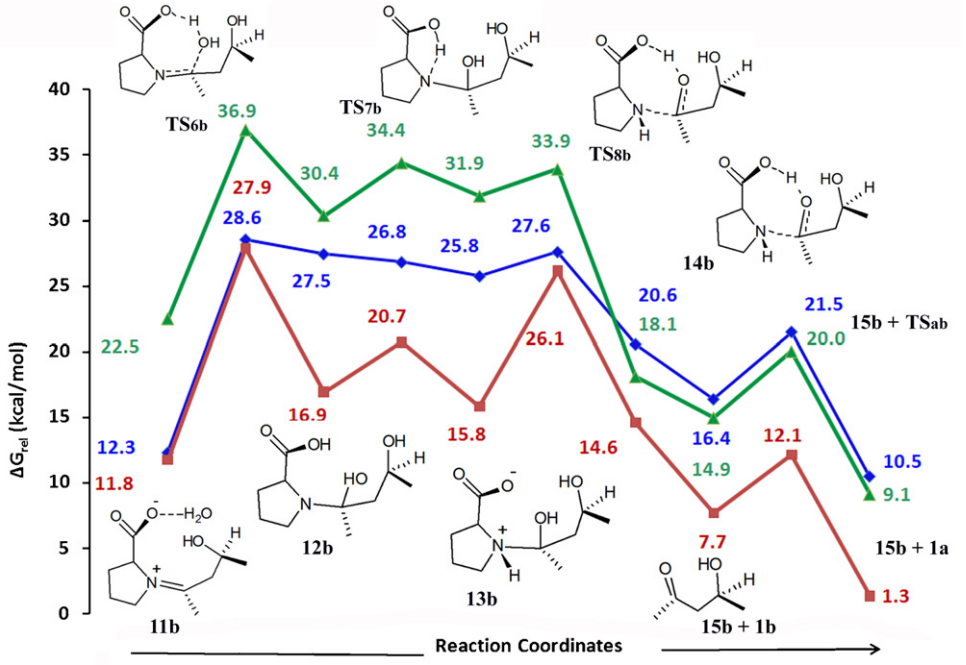

Fig. 7. Energy profile diagram for the regeneration of (*S*)-proline catalyst. The numerical values are the relative Gibbs energies (ΔG_{rel}) in kcal/mol (values of B3LYP-PCM in green, MPWB1K-PCM in red and B97D-PCM in blue colors) with respect to **1a**. (For interpretation of the references to color in this figure legend, the reader is referred to the web version of the article.)

4. Conclusions

In summary, we have reinvestigated the intermolecular aldol reaction of acetone and acetaldehyde catalyzed by (*S*)-proline by different DFT-PCM methods (MPWB1K-PCM/6-31++G(d,p), B3LYP-PCM/6-31G(d,p) and B97D-PCM/6-311+G(d,p) basis sets) and the full catalytic cycle of the reaction yielding the stereoselective product is established on the basis of dispersion-corrected B97D-PCM/6-311+G(d,p) level of theory. All the DFT methods agreed to the conclusion that a higher energy conformation of (*S*)-proline is the active form of the catalyst and not the most stable conformation. Further, the possibility of different diastereomeric transition states was investigated on the basis of relative Gibbs energies. On the basis of the energetics obtained using the three DFT methods, the full catalytic cycle suggested five important steps, *viz.* (i) first nucleophilic addition between catalyst and acetone via **TS_{1b}**, (ii) iminium ion formation via **TS_{3b}**, (iii) imine–enamine conversion via **TS_{4b}**, (iv) C–C bond formation via **TS_{5b}**, (v) water addition via **TS_{6b}**. The ΔG_{rel} for the ordered quintet (**TS_{1b}**, **TS_{3b}**, **TS_{4b}**, **TS_{5b}**, **TS_{6b}**) at B3LYP-PCM/6-31G(d,p) level is (26.0, 28.1, 30.0, 37.1, 36.9 kcal/mol), at MPWB1K-PCM/6-31++G(d,p) level is (25.6, 24.8, 24.5, 29.6, 27.9 kcal/mol) and at B97D-PCM/6-311+G(d,p) level is (17.1, 18.0, 15.9, 19.9, 28.6 kcal/mol) whereas the $\Delta G^{\#}$ calculated with respect to infinitely separated reactants for the ordered quintet (**TS_{1b}**, **TS_{3b}**, **TS_{4b}**, **TS_{5b}**, **TS_{6b}**) at B3LYP-PCM/6-31G(d,p) level is (20.1, 9.9, 11.8, 16.0, 14.8 kcal/mol), at MPWB1K-PCM/6-31++G(d,p) level is (19.3, 13.6, 16.3, 16.3, 21.4 kcal/mol) and at B97D-PCM/6-311+G(d,p) level is (11.2, 3.5, 16.2, 10.4, 21.7 kcal/mol). The ΔG_{rel} values indicate that structures calculated with dispersion-corrected method are substantially more stable than those with other methods. On the other hand, the B3LYP-PCM method clearly underestimates the stability of the intermediates and transition states. On the basis of the $\Delta G^{\#}$ values obtained at B97D-PCM and MPWB1K-PCM levels, it can be said that the water addition (**TS_{6b}**) is the most difficult step of the catalytic cycle. According to the B97D-PCM results, the second most difficult step of the catalytic cycle has to be the imine to enamine conversion (**TS_{4b}**). The C–C bond formation and imine to enamine conversion steps have nearly equal $\Delta G^{\#}$ at MPWB1K-PCM level while the B97D-PCM results showed that C–C bond formation is a relatively easy step. Previous studies supported the imine to enamine conversion as the rate determining step in proline catalyzed intramolecular aldol reaction [84]. On the other hand, kinetic and mechanistic studies of intermolecular aldol reaction by Blackmond et al. [48] suggested that the rate limiting step is the C–C bond formation. The results presented herein suggest that water addition is the most difficult step of the catalytic cycle which may find support in the experimental findings of Pihko et al. [85,86] where they report that water in stoichiometric conditions (100–500%) both speeded up the reaction and increased the enantioselectivity. A noteworthy feature of the reaction is that the amine and carboxylate functionality operated in tandem for the proton migration in almost every step of the reaction through the formation of hydrogen bonds, and thus the (*S*)-proline catalyzed aldol reaction may be categorized under the hydrogen bond catalysis. In fact, it is felt that this type of hydrogen bond catalysis can play an important role in certain enzymatic reactions, particularly when carboxyl functionality of the amino acids concentrates in the active region [54]. This study adds new insights into our understanding of aldol reaction in terms of the conformational choice of the proline catalyst, Gibbs energy profile, proton relay mechanism and the determination of the rate limiting steps.

Acknowledgments

This research is supported by Council of Scientific and Industrial Research (CSIR), India. A.M.J. is thankful to UGC, Government of India for providing research fellowship. The authors are also thankful to Prof. G. Frenking for fruitful discussions.

Appendix A. Supplementary data

Supplementary data associated with this article can be found, in the online version, at doi:10.1016/j.molcata.2011.05.016.

References

[1] B.R. Buckley, Annu. Rep. Prog. Chem., Sect. B: Org. Chem. 104 (2008) 88–105.
[2] P.I. Dalko, L. Moisan, Angew. Chem., Int. Ed. 43 (2004) 5138–5175.
[3] D.W.C. MacMillan, Nature 455 (2008) 304–308.
[4] S. Mukherjee, J.W. Yang, S. Hoffmann, B. List, Chem. Rev. 107 (2007) 5471–5569.
[5] W. Notz, F. Tanaka, C.F. Barbas III, Acc. Chem. Res. 37 (2004) 580–591.
[6] B. List, Chem. Rev. 107 (2007) 5413–5415.
[7] H. Pellissier, Tetrahedron 63 (2007) 9267–9331.
[8] K.N. Houk, B. List, Acc. Chem. Res. 37 (2004) 487.
[9] A. Dondoni, A. Massi, Angew. Chem., Int. Ed. 47 (2008) 4638–4660.
[10] C.F. Barbas III, Angew. Chem., Int. Ed. 47 (2008) 42–47.
[11] Y. Hayashi, J. Synth. Org. Chem. Jpn. 63 (2005) 464–473.
[12] B. List, Synlett (2001) 1675–1686.
[13] D. Enders, C. Grondal, M.R.M. Hüttl, Angew. Chem., Int. Ed. 46 (2007) 1570–1581.
[14] B. List, R.A. Lerner, C.F. Barbas III, J. Am. Chem. Soc. 122 (2000) 2395–2396.
[15] B. List, Tetrahedron 58 (2002) 5573–5590.
[16] B. List, L. Hoang, H.J. Martin, Proc. Natl. Acad. Sci. U.S.A 101 (2004) 5839–5842.
[17] T. Hoffmann, G. Zhong, B. List, D. Shabat, J. Anderson, S. Gramatikova, R.A. Lerner, C.F. Barbas III, J. Am. Chem. Soc. 120 (1998) 2768–2779.
[18] M. Gruttadauria, F. Giacalone, R. Noto, Chem. Soc. Rev. 37 (2008) 1666–1688.
[19] Z.G. Hajos, D.R. Parrish, J. Org. Chem. 39 (1974) 1615–1621.
[20] U. Eder, G. Sauer, R. Wiechert, Angew. Chem., Int. Ed. 10 (1971) 496–497.
[21] E. Lacoste, Synlett (2006) 1973–1974.
[22] K. Sakthivel, W. Notz, T. Bui, C.F. Barbas III, J. Am. Chem. Soc. 123 (2001) 5260–5267.
[23] C. Agami, J. Levisalles, C. Puchot, J. Chem. Soc., Chem. Commun. (1985) 441–442.
[24] C. Agami, C. Puchot, H. Sevestre, Tetrahedron Lett. 27 (1986) 1501–1504.
[25] F.R. Clemente, K.N. Houk, Angew. Chem., Int. Ed. 43 (2004) 5766–5768.
[26] P.H.Y. Cheong, K.N. Houk, Synthesis (2005) 1533–1537.
[27] S. Bahmanyar, K.N. Houk, J. Am. Chem. Soc. 123 (2001) 12911–12912.
[28] S. Bahmanyar, K.N. Houk, J. Am. Chem. Soc. 123 (2001) 11273–11283.
[29] F.R. Clemente, K.N. Houk, J. Am. Chem. Soc. 127 (2005) 11294–11302.
[30] Y. Li, M.N. Paddon-Row, K.N. Houk, J. Am. Chem. Soc. 110 (1988) 3684–3686.
[31] L. Hoang, S. Bahmanyar, K.N. Houk, B. List, J. Am. Chem. Soc. 125 (2003) 16–17.
[32] M.E. Jung, Tetrahedron 32 (1976) 3–31.
[33] K.N. Rankin, J.W. Gauld, R.J. Boyd, J. Phys. Chem. A 106 (2002) 5155–5159.
[34] F. Ban, K.N. Rankin, J.W. Gauld, R.J. Boyd, Theor. Chem. Acc. 108 (2002) 1–11.
[35] M. Arno, L.R. Domingo, Theor. Chem. Acc. 108 (2002) 232–239.
[36] S. Bahmanyar, K.N. Houk, H.J. Martin, B. List, J. Am. Chem. Soc. 125 (2003) 2475–2479.
[37] C. Allemann, R. Gordillo, F.R. Clemente, P.H.Y. Cheong, K.N. Houk, Acc. Chem. Res. 37 (2004) 558–569.
[38] S. Bahmanyar, K.N. Houk, Org. Lett. 5 (2003) 1249–1251.
[39] C. Allemann, J.M. Um, K.N. Houk, J. Mol. Catal. A: Chem. 324 (2010) 31–38.
[40] A.K. Sharma, R.B. Sunoj, Angew. Chem., Int. Ed. 49 (2010) 6373–6377.
[41] C.B. Shinisha, R.B. Sunoj, Org. Biomol. Chem. 5 (2007) 1287–1294.
[42] G. Yang, Z. Yang, L. Zhou, R. Zhu, C. Liu, J. Mol. Catal. A: Chem. 316 (2010) 112–117.
[43] F.J.S. Duarte, E.J. Cabrita, G. Frenking, A.G. Santos, J. Org. Chem. 75 (2010) 2546–2555.
[44] A. Fu, H. Li, F. Tian, S. Yuan, H. Si, Y. Duan, Tetrahedron Asymmetry 19 (2008) 1288–1296.
[45] P. Hammar, C. Ghobril, C. Antheaume, A. Wagner, R. Baati, F. Himo, J. Org. Chem. 75 (2010) 4728–4736.
[46] X.Y. Xu, Z. Tang, Y.Z. Wang, S.W. Luo, L.F. Cun, L.Z. Gong, J. Org. Chem. 72 (2007) 9905–9913.
[47] M.B. Schmid, K. Zeitler, R.M. Gschwind, Angew. Chem., Int. Ed. 49 (2010) 4997–5003.
[48] N. Zotova, L.J. Broadbelt, A. Armstrong, D.G. Blackmond, Bioorg. Med. Chem. Lett. 19 (2009) 3934–3937.
[49] N. Zotova, A. Franzke, A. Armstrong, D.G. Blackmond, J. Am. Chem. Soc. 129 (2007) 15100–15101.
[50] J. Díaz, J.M. Goodman, Tetrahedron 66 (2010) 8021–8028.
[51] A. Lesarri, S. Mata, E.J. Cocinero, S. Blanco, J.C. López, J.L. Alonso, Angew. Chem., Int. Ed. 41 (2002) 4673–4676.
[52] S. Mata, V. Vaquero, C. Cabezas, I. Pena, C. Perez, J.C. Lopez, J.L. Alonso, Phys. Chem. Chem. Phys. 11 (2009) 4141–4144.
[53] U. Pidun, G. Frenking, Chem. Eur. J. 4 (1998) 522–540.
[54] D. Rothlisberger, O. Khersonsky, A.M. Wollacott, L. Jiang, J. DeChancie, J. Betker, J.L. Gallaher, E.A. Althoff, A. Zanghellini, O. Dym, S. Albeck, K.N. Houk, D.S. Tawfik, D. Baker, Nature 453 (2008) 190–195.
[55] A.D. Becke, J. Chem. Phys. 98 (1993) 5648–5652.
[56] C. Lee, W. Yang, R.G. Parr, Phys. Rev. B 37 (1988) 785–789.
[57] K.S. Krishnan, J.M. Kuthanappillil, J. John, C.H. Suresh, E. Suresh, K.V. Radhakrishnan, Synthesis (2008) 2134–2140.
[58] A.N. Pillai, C.H. Suresh, V. Nair, Chem. Eur. J. 14 (2008) 5851–5860.
[59] C.H. Suresh, D. Ramaiah, M.V. George, J. Org. Chem. 72 (2007) 367–375.
[60] Y. Zhao, D.G. Truhlar, Acc. Chem. Res. 41 (2008) 157–167.
[61] M.D. Wodrich, C. Corminboeuf, P.V.R. Schleyer, Org. Lett. 8 (2006) 3631–3634.
[62] Y. Zhao, D.G. Truhlar, J. Phys. Chem. A 108 (2004) 6908–6918.
[63] N. Mohan, K.P. Vijayalakshmi, N. Koga, C.H. Suresh, J. Comput. Chem. 31 (2010) 2874–2882.
[64] C.H. Suresh, N. Mohan, K.P. Vijayalakshmi, R. George, J.M. Mathew, J. Comput. Chem. 30 (2009) 1392–1404.
[65] S. Grimme, J. Comput. Chem. 27 (2006) 1787–1799.
[66] R. Peverati, K.K. Baldridge, J. Chem. Theor. Comput. 4 (2008) 2030–2048.
[67] R.A. Moss, L. Wang, C.M. Odorisio, K. Krogh-Jespersen, J. Am. Chem. Soc. 132 (2010) 10677–10679.
[68] L. Ducháčková, A. Kadlčíková, M. Kotora, J. Roithová, J. Am. Chem. Soc. 132 (2010) 12660–12667.
[69] A. Kadlčíková, I. Valterová, L. Ducháčková, J. Roithová, M. Kotora, Chem. Eur. J. 16 (2010) 9442–9445.
[70] B. Mennucci, R. Cammi, J. Tomasi, J. Chem. Phys. 110 (1999) 6858–6870.
[71] M. Cossi, G. Scalmani, N. Rega, V. Barone, J. Chem. Phys. 117 (2002) 43–54.
[72] M.J. Frisch, G.W. Trucks, H.B. Schlegel, G.E. Scuseria, M.A. Robb, J.R. Cheeseman, J.A.T.V. Montgomery Jr., K.N. Kudin, J.C. Burant, J.M. Millam, S.S. Iyengar, J. Tomasi, V. Barone, B. Mennucci, M. Cossi, G. Scalmani, N. Rega, G.A. Petersson, H. Nakatsuji, M. Hada, M. Ehara, K. Toyota, R. Fukuda, J. Hasegawa, M. Ishida, T. Nakajima, Y. Honda, O. Kitao, H. Nakai, M. Klene, X. Li, J.E. Knox, H.P. Hratchian, J.B. Cross, C. Adamo, J. Jaramillo, R. Gomperts, R.E. Stratmann, O. Yazyev, A.J. Austin, R. Cammi, C. Pomelli, J.W. Ochterski, P.Y. Ayala, K. Morokuma, G.A. Voth, P. Salvador, J.J. Dannenberg, V.G. Zakrzewski, S. Dapprich, A.D. Daniels, M.C. Strain, O. Farkas, D.K. Malick, A.D. Rabuck, K. Raghavachari, J.B. Foresman, J.V. Ortiz, Q. Cui, A.G. Baboul, S. Clifford, J. Cioslowski, B.B. Stefanov, G. Liu, A. Liashenko, P. Piskorz, I. Komaromi, R.L. Martin, D.J. Fox, T. Keith, M.A. Al-Laham, C.Y. Peng, A. Nanayakkara, M. Challacombe, P.M.W. Gill, B. Johnson, W. Chen, M.W. Wong, C. Gonzalez, J.A. Pople, Gaussian 03, Revision D.02, Gaussian, Inc., Wallingford CT, 2004.
[73] M.J. Frisch, G.W. Trucks, H.B. Schlegel, G.E. Scuseria, M.A. Robb, J.R. Cheeseman, G.B.V. Scalmani, B. Mennucci, G.A. Petersson, H. Nakatsuji, M. Caricato, X. Li, H.P. Hratchian, A.F. Izmaylov, J. Bloino, G. Zheng, J.L. Sonnenberg, M. Hada, M. Ehara, K. Toyota, R. Fukuda, J. Hasegawa, M. Ishida, T. Nakajima, Y. Honda, O. Kitao, H. Nakai, T. Vreven, J.J.A. Montgomery, J.E. Peralta, F. Ogliaro, M. Bearpark, J.J. Heyd, E. Brothers, K.N. Kudin, V.N. Staroverov, R. Kobayashi, J. Normand, K. Raghavachari, A. Rendell, J.C. Burant, S.S. Iyengar, J. Tomasi, M. Cossi, N. Rega, N.J. Millam, M. Klene, J.E. Knox, J.B. Cross, V. Bakken, C. Adamo, J. Jaramillo, R. Gomperts, R.E. Stratmann, O. Yazyev, A.J. Austin, R. Cammi, C. Pomelli, J.W. Ochterski, R.L. Martin, K. Morokuma, V.G. Zakrzewski, G.A. Voth, P. Salvador, J.J. Dannenberg, S. Dapprich, A.D. Daniels, Ö. Farkas, J.B. Foresman, J.V. Ortiz, J. Cioslowski, D.J. Fox, Gaussian 09, Revision A.1, Gaussian, Inc., Wallingford CT, 2009.
[74] C.Y. Peng, H.B. Schlegel, Isr. J. Chem. 33 (1993) 449–454.
[75] C.Y. Peng, P.Y. Ayala, H.B. Schlegel, M.J. Frisch, J. Comput. Chem. 17 (1996) 49–56.
[76] F. Calderon, E.G. Doyaguez, P.H.-Y. Cheong, A. Fernandez-Mayoralas, K.N. Houk, J. Org. Chem. 73 (2008) 7916–7920.
[77] T.A. Spencer, H.S. Neel, T.W. Flechtner, R.A. Zayle, Tetrahedron Lett. 6 (1965) 3889–3897.
[78] H. Molines, C. Wakselman, Tetrahedron 32 (1976) 2099–2103.
[79] H.B. Burgi, J.D. Dunitz, Acc. Chem. Res. 16 (1983) 153–161.
[80] H.B. Burgi, J.D. Dunitz, J.M. Lehn, G. Wipff, Tetrahedron 30 (1974) 1563–1572.
[81] H.B. Burgi, J.D. Dunitz, E. Shefter, J. Am. Chem. Soc. 95 (1973) 5065–5067.
[82] Y. Hayashi, W. Tsuboi, M. Shoji, N. Suzuki, Tetrahedron Lett. 45 (2004) 4353–4356.
[83] S. Chandrasekhar, N.R. Reddy, S.S. Sultana, C. Narsihmulu, K.V. Reddy, Tetrahedron 62 (2006) 338–345.
[84] H. Zhu, F.R. Clemente, K.N. Houk, M.P. Meyer, J. Am. Chem. Soc. 131 (2009) 1632–1633.
[85] A.I. Nyberg, A. Usano, P.M. Pihko, Synlett (2004) 1891–1896.
[86] P.M. Pihko, K.M. Laurikainen, A. Usano, A.I. Nyberg, J.A. Kaavi, Tetrahedron 62 (2006) 317–328.